Study of the eclipse region of the redback millisecond pulsar J1431–4715

IOP Conf. Series: Journal of Physics: Conf. Series **956** (2018) 012004 doi:10.1088/1742-6596/956/1/012004

Study of the eclipse region of the redback millisecond pulsar J1431−4715

A Miraval Zanon[1], M Burgay[2], A Possenti[2] and A Ridolfi[3]

[1] Dipartimento di Fisica e Astronomia "Galileo Galilei" - Università di Padova, Vicolo dell'Osservatorio 3, Padova, IT-35122, Italy
[2] Osservatorio Astronomico di Cagliari, INAF, Via della Scienza 5, I-09047 Selargius (CA), Italy
[3] Max-Planck-Institut für Radioastronomie, Auf dem Hügel 69, D-53121 Bonn, Germany

E-mail: arianna.miravalzanon@studenti.unipd.it

Abstract. We report on the rotational, astrometric and orbital parameters for PSR J1431−4715, and we also present a preliminary analysis of the eclipsing region. This pulsar was discovered in the High Time Resolution Universe survey and it belongs to the class of "redback" systems. The minimum estimated mass for the companion of J1431−4715 is, indeed, 0.13 $M_\odot$. Thanks to multi-frequency observations, obtained at the 64 m Parkes radio telescope, we note that the magnitude and the duration of the eclipse delay depend upon the observing frequency.

1. Introduction

MilliSecond pulsars (MSPs) are a population of Neutron Stars (NSs) with fast spin (hundreds of rotations per second) and relatively weak magnetic field (10^8 G).
These objects are thought to be generated in Low-Mass X-ray Binary systems (LMXBs), where a NS is spun up by the accretion of matter and angular momentum from its companion [1]. This process is called "recycling" and the pulsars that have experienced it are dubbed "recycled" pulsars. The X-ray emission of LMXBs is actually powered by this accretion.
According to the current theory, the progenitors of MSPs are bright X-ray binaries, in which a luminous main sequence star overflows its Roche lobe and transfers mass to the NS. Tidal forces during the mass transfer circularize the orbit, while the original companion star loses matter and typically becomes a white dwarf.
Among MSPs, the so-called "eclipsing binary millisecond pulsars" emit a radio signal that is distorted or completely disappears, at some particular orbital phases. There are two sub-populations of eclipsing MSPs: Black Widow (BW) and RedBack (RB) pulsars. BWs have very low-mass companions ($M_2 \leq 0.1$ $M_\odot$), while RBs have slightly heavier companions ($M_2 \simeq 0.1 - 0.4$ $M_\odot$). In the former type, the companion star is a largely ablated degenerate star; in the latter type, the companion is non-degenerate and only partially ablated.
The discovery of BW and RB systems has highlighted the link between LMXBs and recycled binary radio pulsars. Recent observations (e.g. [2]) confirmed the transition between an accretion-powered state (in which the system is a LMXB and bright X-ray emission is observed) and a rotation-powered state (in which radio emission is powered by the NSs rotating magnetic field) for some RB systems.

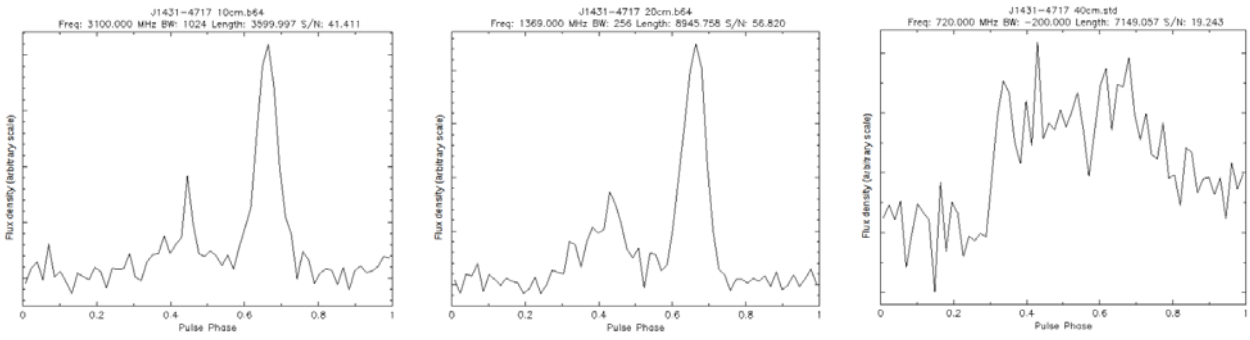

Figure 1. Starting from the left, integrated pulse profile of PSR J1431−4715 at 3.1 GHz, 1.4 GHz and 0.7 GHz.

Observations of the eclipse regions of BWs and RBs show that the radio pulsed signal is delayed, distorted or completely absorbed by a low-dense, highly ionized gas cloud enshrouding the companion. This eclipsing material can be originated by the companion star being hit by the pulsar's high-energy wind [3]. Alternatively, the eclipsing material could come from an accretion disk whose flow of matter is stopped and blown away by the MSP's radiation pressure at the inner Lagrangian point [4].

2. Observations and analysis

PSR J1431−4715 was discovered in the High Time Resolution Universe (HTRU) survey [5] with the 64 m Parkes radio telescope using the 13 beam 21 cm multibeam receiver, observing the intermediate Galactic latitude regions ($-120° < l < 30°, \mid b \mid \leq 15°$).

Our dataset consisted of observations made with the Parkes radio telescope from 2011 July to 2017 June. The pulsar was regularly observed in this time interval with different backends: APSR (Australia Telescope National Facility Parkes Swinburne Recorder), CASPSR (Center for Astronomy Signal Processing and Electronics Research Parkes Swinburne Recorder) and DFB3/4 (Digital Filterbank) [6]. Most of the observations were made at 1.4 GHz, while some others were made simultaneously at 0.7 GHz and 3.1 GHz with the coaxial 10/50 cm receiver. The pulsar is well visible at 1.4 GHz and 3.1 GHz, while the signal at 0.7 GHz is very noisy.

The pulsar signal, crossing the InterStellar Medium (ISM), suffers frequency-dependent delays due to the effects of dispersion (for more details see [7]). These delays can be corrected with a procedure called de-dispersion, which is based on the knowledge of the Dispersion Measure (DM). The DM represents the electron column density along the source line of sight and can be expressed as:

$$\mathrm{DM} = \int_0^d n_e(l)\mathrm{d}l, \tag{1}$$

where n_e is the electron density along the path, d is the source distance with respect to the Earth. Dispersion occurs because the group velocity of electromagnetic waves through an ionized medium is frequency dependent. Radiation at higher frequencies travels faster than radiation at lower frequencies.

In the observations that we analyzed the signal is acquired in *folding mode*. When folding, the observing band is first divided into a number of channels and in each one the effect of dispersion is removed according to the value of the DM. After de-dispersing, the observation is divided into subsequent time intervals, called sub-integrations. Each sub-integration is summed in phase according to the pulsar spin period, in order to form an integrated profile. This observing mode

is used when the basic characteristics of the pulsar are known, as in our case. The folding procedure allows us to sum many pulses in order to make the signal visible over the background noise.
The aim of our analysis was mainly to measure with high accuracy the astrometric, rotational and orbital parameters of PSR J1431−4715, using a procedure called *timing*.
Using the `PSRCHIVE` pulsar software [8], we have extracted the topocentric times-of-arrival (ToAs) by cross-correlating each integrated pulse profile with a high signal-to-noise (S/N) template profile. Template profiles at three different frequencies are shown in Fig. 1; these were obtained by coherently summing our best detections. Multi-frequency observations show a significant pulse profile evolution: pulse profiles at 3.1 GHz and 1.4 GHz are doubled peaked, while the pulse profile at 0.7 GHz is broadened and noisy.
We used the `TEMPO2` pulsar timing package [9] in order to convert the topocentric ToAs, t_i, to the barycentric ToAs $t_{i,bary}$, referred to the Solar System Barycenter (SSB), with the formula:

$$t_{i,bary} = t_i + t_{clock} - \frac{D(t_i)}{f^2} + \Delta R_\odot + \Delta E_\odot + \Delta S_\odot, \tag{2}$$

where t_{clock} is the clock correction chain, $D(t_i)$ is the delay due to interstellar dispersion, $\Delta R_\odot$ is the Roemer delay, $\Delta E_\odot$ is the Einstein delay and $\Delta S_\odot$ is the Shapiro delay.
In our case the pulsar is in a binary system, so before translating the ToAs expressed in pulsar proper time at the pulsar surface to the SSB, we must calculate them at the Pulsar Binary Barycenter.
The aim of the timing procedure is to find the parameters that correctly describe the rotation of our pulsar by accounting for every single rotation of the NS in a given time window. To do so, `TEMPO2` models the rotational evolution of the neutron star with a Taylor expansion of the number of rotations:

$$N(t) = \nu_{ep}(t - t_{ep}) + \frac{1}{2}\dot{\nu}_{ep}(t - t_{ep})^2 + \frac{1}{6}\ddot{\nu}_{ep}(t - t_{ep})^3 + ..., \tag{3}$$

where ν_{ep}, $\dot{\nu}_{ep}$, $\ddot{\nu}_{ep}$ are neutron star spin frequency, the first and second derivative of the spin frequency at a reference epoch t_{ep}. $N(t)$ represents the number of rotations occurred from t_{ep} to t.
Using again `TEMPO2` we examined the so-called *timing residuals*, i.e. the differences between the observed ToAs and the values predicted by our model. In order to derive the best timing solution we have minimized the weighted χ^2 for the astrometric, rotational and orbital parameters. The best-fitting timing parameters for J1431−4715 are reported in Tab. 1. Thanks to the large time span of our dataset, we were able to measure the orbital period derivative $\dot{P}_b$. We performed an F-test to determine if the addition of $\dot{P}_b$ was indeed required by the data. Without it, $\chi^2 = 440$ with 60 degrees of freedom, while after fitting for $\dot{P}_b$ the χ^2 improved to 71.12 with 70 degrees of freedom. A negative $\dot{P}_b$ indicates a gravitational energy loss by the system, but the contribution to $\dot{P}_b$ expected from General Relativity (GR) is three orders of magnitude smaller than observed, assuming $M_p = 1.4$ $M_\odot$ and $M_c = M_{c,\min}$. The value found for $\dot{P}_b$ with timing analysis is probably due to mass loss from the companion star. This lost matter is ejected from the system due to the pulsar wind and leads to a decrease of the angular momentum and the orbital period of the system.
The timing residuals shown in the left plot of Fig. 2, as a function of Modified Julian Day, (MJD), do not show any structure but are randomly distributed. This is indicative of the fact that the best-fitting timing model is correctly describing the pulsar's behaviour. The right plot in Fig. 2 shows the timing residuals as a function of frequency, used for a precise determination of the DM value. For this measure we used observations at three different frequencies because

the delay in the ToAs inversely depends on the square of the observing frequency as

$$\Delta t = \frac{e^2}{2\pi m_e c}\mathrm{DM}\left(\frac{1}{f_{min}^2} - \frac{1}{f_{max}^2}\right). \tag{4}$$

From Eq. (4), knowing from the observations the time delay in the ToAs (Δt) and the observing frequencies (f_{min} and f_{max}), we can measure the DM value. The larger the $f_{min} - f_{max}$ difference, the more precise the DM determination is.

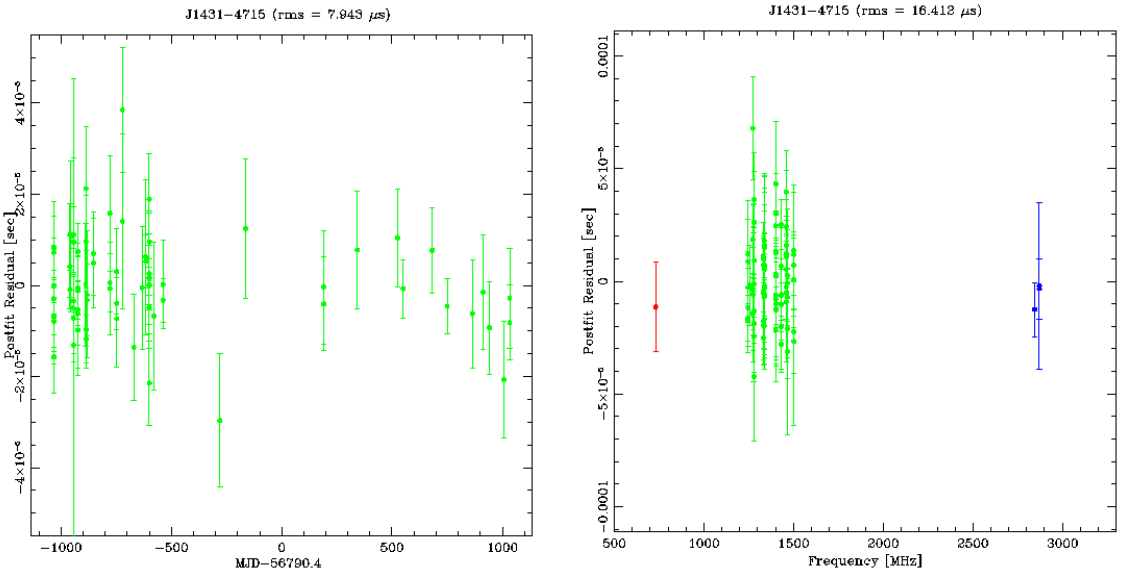

Figure 2. Left plot: timing residuals of J1431−4715 for observations at 1.4 GHz when fitting for all the parameters but the DM. Right plot: timing residuals of J1431−4715 with observations at 0.7 GHz (red), 1.4 GHz (green) and 3.1 GHz (blue) when fitting for the DM.

3. Results

From the measured parameters we can also determine, with some assumptions, other characteristics of the system. One of these is the mass function, defined as

$$f(M_p) = \frac{4\pi^2}{G}\frac{x_p^3}{P_b^2} = \frac{(M_c \sin i)^3}{(M_p + M_c)^2}, \tag{5}$$

where G is the gravitational constant, x_p is the projected semi-major axis of the pulsar orbit, P_b is the orbital period, M_p is the mass of the pulsar, M_c is the companion's mass and i is the inclination of the system (i.e. the angle between the line of sight and the normal to the orbital plane). From the mass function we estimated the minimum companion mass to be 0.13 $\mathrm{M}_\odot$ (see Tab. 1), assuming $M_p = 1.4$ $\mathrm{M}_\odot$ and $i = 90°$.

Finally, assuming that the emission of the pulsar is solely due to the rotational energy loss in the form of magneto-dipole radiation, we estimated the surface dipolar magnetic field, B_0, and the so-called characteristic age, τ_c, as

$$B_0 \approx 3.2 \times 10^{19}\mathrm{G}\sqrt{P\dot{P}}, \qquad \tau_c \approx \frac{P}{2\dot{P}}. \tag{6}$$

The values found are: $B_0 = 1.69 \times 10^8$ G, $\tau_c = 2.25$ Gyr. Some parameters (namely μ_α, μ_δ, DM, x_p and $\dot{P}$) are now measured with higher precision compared to previously published values (see Tab. 1). The other parameters have roughly the same errors of [11].

Pulsar	J1431−4715
Right Ascension, α (J2000)	14:31:44.6182(1)
Declination, δ (J2000)	−47:15:27.567(2)
Proper Motion in α, μ_α (mas yr^{-1})	−11.0(8)
Proper Motion in δ, μ_δ (mas yr^{-1})	−14.2(8)
Spin Frequency, f (s^{-1})	497.02939385196(6)
1st Spin Frequency derivative, $\dot{f}$ (Hz s^{-2})	$-3.4949(7)\times10^{-15}$
Reference Epoch (MJD)	55756.100
Start of Timing Data (MJD)	55758.264
End of Timing Data (MJD)	57845.655
Dispersion Measure, DM (pc cm^{-3})	59.345(2)
Terrestrial Time Standard	TT(TAI)
Time Units	TCB
Number of ToAs	90
Binary Parameters	
Binary Model	ELL1
Projected Semi-major Axis, x_p (lt-s)	0.550053(6)
Epoch of passage at Ascending Node, $T_{\rm asc}$ (MJD)	55756.1047756(4)
Orbital Period, P_b (days)	0.4497391416(7)
Orbital period derivative, $\dot{P}_b$ (10^{-11} s s^{-1})	−1.09(7)
Derived Parameters	
Spin Period, P (s)	$2.0119534425319(2)\times10^{-3}$
1st Spin Period derivative, $\dot{P}$ (s s^{-1})	$1.4147(3)\times10^{-20}$
Mass Function, $f(M_{\rm p})$ (M$_\odot$)	8.83×10^{-4}
Minimum companion mass, $M_{\rm c,min}$ (M$_\odot$)	0.13
Surface Magnetic Field, B_0, (10^8 G)	1.69
Characteristic Age, $\tau_{\rm c}$ (Gyr)	2.25

Table 1. Timing parameters for pulsar J1431−4715. All the uncertainties are the nominal 1-σ values calculated by `TEMPO2`. ELL1 is a binary orbital model particularly suitable for very-low eccentricities [10].

4. Study of the eclipse region

The results in the previous section do not take into account the observations taken during the eclipse phase. The left plot of Fig. 3 shows the timing residuals for all the observations at three different frequencies.

In the orbital phase range between 0.1 and 0.4 (i.e. around superior conjunction, which occurs at phase 0.25) there is a clear delay in the radio signal. Nevertheless, the radio signal never disappears across the eclipse region. The eclipse lasts for about 2.7 h, corresponding to 25% of the orbital period.

We can notice that the delays depend upon observing frequency and in some observations at 3.1 GHz (blue dots) they show smaller delays than 1.4 GHz (green dots).

We assume that the responsible for the eclipse is a low-density highly-ionized gas cloud enwrapping the companion star.

In this case we can suppose that the delay is due to an orbital phase dependent excess of material between the pulsar and the Earth. Indeed, if we convert the time delays into electron column densities (see Fig. 3, right plot), we can see that the difference between observations at 3.1 GHz and 1.4 GHz is removed. We can conclude that these delays are mainly due to additional DM. The associated extra DM does not cause a decrease in the total flux density, but in addition to the delay in the ToAs, it causes smearing. This phenomenon determines a broadening of the

pulse profile due to the rapid variation of the dispersion measure in the eclipse region. The extra contribution $\Delta\mathrm{DM}(\phi)$ to the dispersion measure can be expressed as

$$\Delta\mathrm{DM}(\phi) = \int_{cloud} n_e dl, \tag{7}$$

where the integral is along the gas cloud at the particular orbital phase.

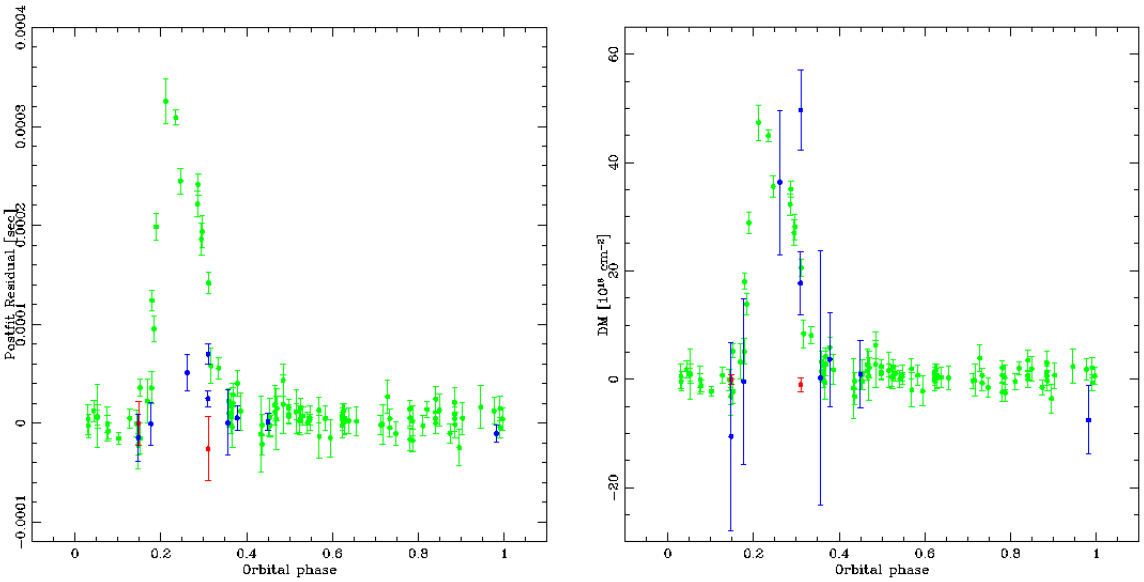

Figure 3. Left plot: ToAs residuals versus orbital phase for J1431−4715 as acquired over a time span of 5 years. The observations were made at 0.7 GHz (red), 1.4 GHz (green) and 3.1 (blue) GHz. Right plot shows the same delays converted to an electron column density.

We can conclude that, as we do not observe a variation in the total flux density, the eclipse in PSR J1431−4715 is not due to absorption processes. Then, the delay is due to the variation of the electron density in the cloud that surrounding the companion star, since that if the delays are converted to an electron column density, the differeces between the delays at 1.4 GHz and 3.1 GHz are removed.

References

[1] Alpar M A, Cheng A F, Ruderman M A and Shaham J 1982 *Nature* **300** 728
[2] Papitto A, Ferrigno C, Bozzo E *et al* 2013 *Nature* **501** 517
[3] van den Heuvel E P J and van Paradijs J 1988 *Nature* **334** 227
[4] Burderi L, D'Antona F, Menna M T *et al* 2001 *X-ray Astronomy 2000* **234** 237
[5] Keith M J, Jameson A, van Straten W *et al* 2010 *MNRAS* **409** 619
[6] Sarkissian J M, Carretti E and van Straten W 2011 *American Institute of Physics Conference Series* **1357** 351
[7] Lorimer D R, Kramer M 2005 *Cambridge University Press* **"Handbook of pulsar Astronomy"**
[8] Hotan A W, van Straten W and Manchester R N 2004 *Publ. Astron. Soc. Australia* **21** 302
[9] Hobbs G B, Edwards R T and Manchester R N 2006 *MNRAS* **369** 655
[10] Lange C, Camilo F, Wex N *et al* 2001 *MNRAS* **326** 274
[11] Bates S D, Thornton D, Bailes M *et al* 2015 *MNRAS* **446** 4019